Current Applied Physics 11 (2011) 1111–1125

Contents lists available at ScienceDirect

Current Applied Physics

journal homepage: www.elsevier.com/locate/cap

Review

Nanoscale studies of defect-mediated polarization switching dynamics in ferroelectric thin film capacitors

Sang Mo Yang [a], Jong-Gul Yoon [b,*], Tae Won Noh [a]

[a] ReCFI, Department of Physics and Astronomy, Seoul National University, Seoul 151-747, Republic of Korea
[b] Department of Physics, University of Suwon, Hwaseong, Gyunggi-do 445-743, Republic of Korea

ARTICLE INFO

Article history:
Received 4 March 2011
Accepted 7 May 2011
Available online 25 May 2011

Keywords:
Ferroelectrics
Polarization
Domain switching
Piezoresponse force microscopy
Defects
Thin films

ABSTRACT

Recent developments in ferroelectric (FE) domain imaging techniques have established an understanding of intriguing polarization switching dynamics. In particular, nanoscale studies of FE domain switching phenomena using piezoresponse force microscopy (PFM) can provide important microscopic details on nucleation and subsequent growth of domains, complementing conventional electrical measurements that only give macroscopic information. This review covers recent nanoscale PFM studies of domain switching dynamics in FE thin films. Recent nanoscale PFM-based studies have demonstrated that quenched defects inside the FE thin films play important roles in domain switching processes, including defect-mediated inhomogeneous nucleation, pinning-dominated nonlinear dynamics of domain walls, and many other intriguing phenomena.

Contents

* Corresponding author. Tel.: +82 31 220 2120; fax: +82 31 220 2517.
E-mail address: jgyoon@suwon.ac.kr (J.-G. Yoon).

1567-1739/$ – see front matter © 2011 Elsevier B.V. All rights reserved.
doi:10.1016/j.cap.2011.05.017

1. Introduction

Since the discovery of ferroelectricity by Valasek in 1920 [1], ferroelectric (FE) materials have been extensively investigated as prototypical material systems that exhibit intriguing phase transition phenomena [2–22]. In FE materials, nonzero electric polarization (P), known as spontaneous polarization (P_S), can appear without an external electric field (E) below a certain critical Curie temperature. Many theoretical and experimental studies have investigated P_S and its instability [2–22]. Pioneering works on the phase transitions of ferroelectricity were carried out by Ginzburg [23] and Devonshire [24] based on the phenomenological Landau mean-field theory [25]. Recently, advances have occurred in many fundamental problems, such as the microscopic origin of ferroelectricity in perovskite-type lattices [5] and critical thickness of ferroelectricity in ultrathin films [6,7,26,27], due to developments of first-principle calculations, fabrication techniques of high-quality FE materials, and so on.

One of the most important problems in FE materials is to understand the switching dynamics of P driven by external E. Ferroelectricity has two peculiarities: the appearance of P_S and the ability to switch between two (or more) P_S states under an external E. When an external E is applied to FE materials, thermodynamically equivalent P_S states become nonequivalent, and the ground state is changed by reversing the P direction. In the 1950s, Merz, Landauer, and several other researchers studied the P switching behavior of single crystals such as $BaTiO_3$ [2,28–34]. Early detailed studies have already been described in several classic books written by Fatuzzo and Merz [2], Lines and Glass [3], and Smolenskii [4].

Recently, the importance of P switching dynamics in FE thin films has been recognized due to their potential applications in numerous multifunctional electronic devices [9–19]. For example, FE thin film capacitors have attracted considerable attention as nonvolatile FE random access memories, FE field-effect transistors, and so on [9–19]. Operation of most FE capacitors-based electronic devices is based on P switching induced by external E. Thus, it is very important to understand the P switching process, in particular, how P switching occurs under an external E in FE materials.

The best way to investigate the P switching process is through direct imaging of domains with sufficient time and spatial resolution. In FE thin film capacitors, P switching is usually completed on the micro- and nanosecond time scales. Additionally, recent developments in the synthesis and fabrication of nanoscale FE structures [11–13,35–37] also require nanoscale resolution for studies of P switching dynamics. However, conventional electrical measurements, such as measurements of P–E hysteresis loops [2–4,31] and transient switching currents [2,38,39], can provide only volume-averaged information on the P switching process, not microscopic images. Conventional optical methods combined with etching techniques provide spatial information on the static and dynamic properties of FE domains [33,34], but they do not have sufficient time resolution to observe the entire P switching process. For these reasons, an understanding of nanoscale P switching dynamics in FE materials is still far from being complete.

In this article, we review recent advances in nanoscale studies of P switching dynamics in FE thin film capacitors. Over the last two decades, new FE domain imaging methods with high spatial and time resolution have been developed. One of the most effective methods is piezoresponse force microscopy (PFM) [37,40–45]. This review emphasizes the remarkable progress in PFM-based experimental studies on FE thin film capacitor geometry. In particular, we highlight the role of defects in FE domain nucleation and growth that were recently revealed due to nanoscale PFM studies. For a comprehensive understanding of the defect-mediated P switching process, we review the basics of P switching in FE materials (Section 2) and discuss numerical models explaining P switching kinetics (Section 3). We compare various PFM-based experimental methods (Section 4) and describe recent results of nanoscale studies on P switching dynamics by PFM (Section 5). We introduce a statistical explanation of the physics of domain wall motion in FE thin films with quenched defects (Section 6). Finally, we discuss several remaining issues and perspectives in nanoscale studies of FE domain switching dynamics (Section 7).

2. *P* switching dynamics in FE materials

2.1. Homogeneous vs. inhomogeneous P switching

Fig. 1a shows an FE material that was initially poled to have the same P directions. In the simplest P switching scenario, the entire FE material switches to the opposite P simultaneously under a certain threshold electric field (intrinsic coercive field, E_{IC} [46]). Such switching is known as homogeneous [47,48] (or intrinsic [49]) P switching. Homogeneous P switching is defined as coherent P reversal at E_{IC} due to instability of the macroscopic P state in an opposing E. In principle, collective P switching can be achieved if a sufficiently high field is applied to an FE material. However, the estimated E_{IC} values, based on Landau mean-field theory [25], are on the order of a few MV/cm or higher in most FE materials. These values are much higher than the experimentally measured coercive field (E_C), typically 100 kV/cm for FE thin films [10]. Thus, in reality, other P switching processes should occur before E reaches E_{IC}.

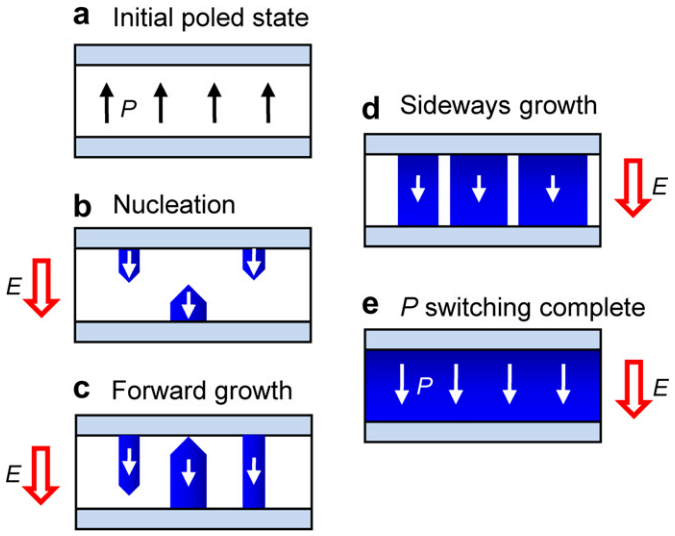

Fig. 1. Schematic of the defect-mediated inhomogeneous polarization (P) switching process induced by an external electric field (E) in a ferroelectric thin film capacitor. (See text for details). (For interpretation of the references to colour in this figure, the reader is referred to the web version of this article).

In most FE systems, *P* switching occurs via creation and subsequent growth of domains with opposite *P* directions. Actually, the free energy of most FE materials generally prefers a configuration consisting of domains in which each *P* is in the same direction, while in adjacent domains, *P* is in the opposite direction [2,3,10,11,50]. It is energetically favorable to switch by nucleation and subsequent growth of a large number of domains (inhomogeneous switching) rather than by simultaneous *P* switching within a domain (homogeneous switching) [10,11]. The low experimental E_C values have been explained using an inhomogeneous [47,48] (or extrinsic [49]) switching mechanism.

Note that a stable domain nucleus should have a finite volume larger than the critical nucleus [10,46,51]. Thus, ultrathin films might limit the nucleus volume, inhibiting the nucleation process. Ducharme et al. reportedly observed homogeneous switching in 1-nm-thick Langmuir–Blodgett polymer ultrathin films [46]. However, this report has been questioned on several points [52], and later work showed that such homogeneous switching is unlikely, even for ultrathin films [53,54]. This indicates that homogeneous switching is highly unlikely in most FE materials of either bulk or thin film form.

2.2. Defect-mediated inhomogeneous P switching process

The first step in inhomogeneous *P* switching is the nucleation of reversed domains in a matrix of opposite *P* (Fig. 1b). In a homogeneous and defect-free material, such nucleation can occur at random positions by a thermally activated process known as homogeneous nucleation. However, it should be noted that homogeneous nucleation cannot occur in most FE materials because unrealistically high energy barriers exist. In the late 1950s, Landauer pointed out that the energy barrier for nucleation (U_N) cannot be overcome using thermal energy, even in the presence of high electric fields: $U_N > 10^8\ k_BT$ at $E \sim 1$ kV/cm (a typical value of E_C for bulk FE) [32] and $U_N > 10^3\ k_BT$ under $E \sim 100$ kV/cm (a typical value of E_C for most FE thin films) [55]. This problem is known as "Landauer's paradox." Many efforts to resolve Landauer's paradox have been made [32,56–62]. To avoid Landauer's paradox, many researchers assumed that nucleation occurs inhomogeneously at particular sites where defects exist [32,56–62]. The existence of defects can reduce the value of U_N, allowing nucleation to occur at such sites.

Here, we note that defects play an important role in FE domain switching dynamics [10,62–64]. Defects control the thermodynamic stability of local *P* states and the kinetic path for *P* switching between thermodynamically equivalent states. Additionally, they act as nucleation centers, as described above, and pinning sites for propagating domain walls, as will be discussed later (Section 6). Typical FE materials enable a broad range of point defects such as oxygen vacancies and extended defects such as dislocations, grain boundaries, defect dipoles, and so on. Therefore, the roles of defects must be considered for a comprehensive understanding of *P* switching dynamics.

Fig. 1 shows how the defect-mediated inhomogeneous *P* switching process can occur under an external *E* in an FE thin film capacitor. Solid (blue) areas and open (red) arrows indicate reversed domains and the applied external *E*, respectively. The first step is domain nucleation (Fig. 1b). As already mentioned, nucleation occurs inhomogeneously due to defects. In FE thin film capacitors, those sites are thought to exist at the FE/electrode interface where local defects frequently occur. Next, the nucleated domains grow rapidly in a needle-like geometry along the applied external *E* direction, namely, across the film (Fig. 1c). This is known as forward growth of domains. When domains complete forward growth, they spread sideways (Fig. 1d). During sideways domain growth, the quenched defects act as pinning centers, preventing the domain wall from propagating. Consequently, the growing domain shape becomes irregular, and domain wall velocity depends significantly on the defect nature. Finally, laterally growing domains merge together, and *P* switching is complete (Fig. 1e).

2.3. Spatial and time scales required for FE domain switching studies

It is essential to investigate FE domain switching phenomena with appropriate spatial and time resolution. Fig. 2 displays the spatial and time scales required for FE domain studies. The solid squares with dashed borderlines indicate the ranges corresponding to domain dynamics and statics in FE thin film capacitors. It should be noted that nucleation time is typically 1 ns in oxide FEs, and the

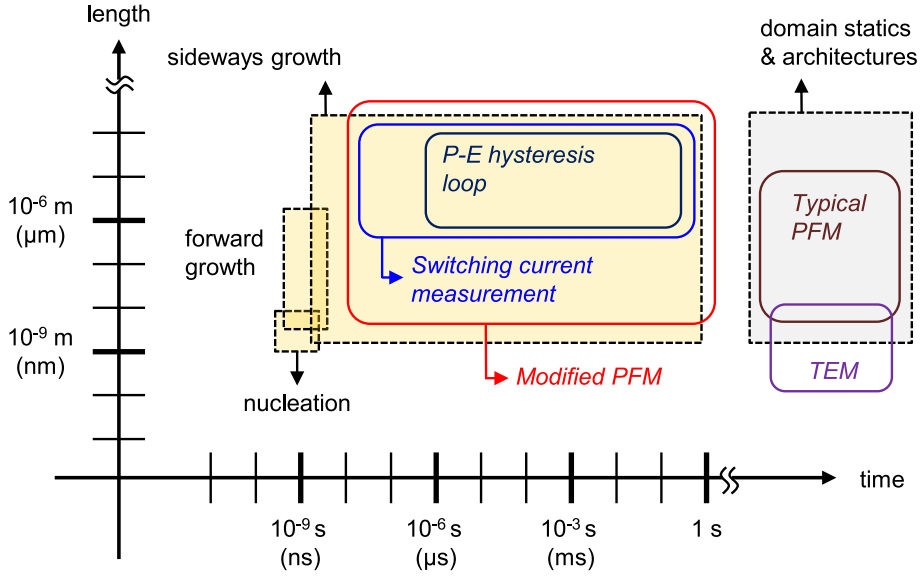

Fig. 2. Spatial and time scales required for FE domain studies. Solid squares with dashed borderlines indicate ranges corresponding to domain dynamics and statics in FE thin film capacitors. Open boxes with solid borderlines indicate the ranges of various experimental methods for FE domain studies.

critical nucleus size is about 1–10 nm [10]. Second, the time required for forward domain growth, $t_{fg} = d/v_{fg}$, where d is film thickness and v_{fg} is the velocity of forward growth, is approximately 1 ns for a few microns-thick film because v_{fg} is typically the speed of sound, a few km/s [10]. The length scale of forward growth corresponds to d because the external field is usually applied in the direction normal to the film surface (c-direction). Third, the velocity of sideways growth depends strongly on the magnitude of the external E, temperature T, film thickness d, defect nature of FE films, and many other conditions [10,28–30,65,66]. Thus, sideways growth time varies from a few nanoseconds to several milliseconds or longer. The spatial range of sideways domain growth varies from the critical nuclei size (a few nm) to the lateral size of the samples. On the other hand, FE domain statics, such as domain structure at the equilibrium state, are primarily related to longer time scales, greater than 1 s, and the spatial range is comparable to that of domain dynamics. Note that the spatial and time scales are extremely broad; thus, it is quite challenging to probe the P switching process with appropriate spatial and time resolution.

2.4. Limitations of conventional methods and new advances in experimental techniques

Due to the spatial and time scales necessary for studying domain dynamics, conventional experimental methods are limited in their ability to characterize FE domain dynamics on the nanoscale. Open boxes with solid borderlines in Fig. 2 show the possible probing ranges of various experimental methods for FE domain studies. Measurements of P–E hysteresis loops, used to derive the values of P_S and E_C, have been used to investigate ac dynamics of FE domain switching behavior [31,67–70]. Although P–E hysteresis loops provide time (t)-dependent information for domain dynamics, they do not provide any spatial information on domain switching, for instance, how and where nuclei are created or how domain walls grow sideways. Transient switching current measurements, which measure the writing pulse width dependence of switched polarization, $\Delta P(t)$, have also been performed to investigate domain switching kinetics [38,39,56,66,71–73]. The time resolution of switching current measurements depends on the minimum width of switching pulses; thus, switching kinetics can be probed at a resolution of 10 ns. However, it is difficult to obtain microscopic details of FE domain switching. On the other hand, transmission electron microscopy (TEM) [64,74,75] and typical PFM [40–42,76–78] provide high spatial resolution of static domain images, domain structures, and long time-relaxation behavior of domains. However, it is difficult to obtain sufficient time resolution of images of FE domain evolution on the nanosecond scale.

Recently, technological breakthroughs have occurred in new experimental methods for studying nanoscale domain dynamics, such as interrupted-switching PFM [79,80] and time-resolved X-ray microdiffraction imaging [81,82]. Interrupted-switching PFM is the most effective method for investigating defect-mediated domain dynamics in FE capacitors with both nanoscale spatial and time resolution, overcoming the time resolution problem of PFM by imaging subsequent snapshots of domain configurations during P switching in FE capacitors step by step [45,79,80]. The time resolution of the interrupted-switching PFM method is determined by the rise time and width of the switching pulses and can be on the order of 10 ns. Furthermore, a modified-PFM technique, combining interrupted-switching PFM with switching current measurements, was developed [58,80]. This allows determination of the reliability of the obtained PFM images during FE domain growth by comparing them with data from separate switching current measurements. As shown in Fig. 2, the modified-PFM technique covers most of the probing ranges necessary for studying domain dynamics in FE thin films. We discuss experimental details of modified PFM and corresponding experimental results in Sections 4.2 and 5, respectively.

3. Numerical models for FE domain switching kinetics

3.1. Kolmogorov–Avrami–Ishibashi (KAI) model

Before describing recent PFM studies on nanoscale FE domain dynamics, we first summarize various numerical models for FE domain switching kinetics. Many numerical models have been developed to explain domain switching kinetics of FE materials. Among them, the statistical model proposed by Kolmogorov [83] and Avrami [84] and extended to FE materials by Ishibashi [38], called the KAI model, has been widely accepted. The KAI model is based on the classical statistical theory of nucleation and unrestricted domain growth based on phase transformation. It assumes that a large number of nuclei become randomly distributed over volume and time. Additionally, it takes into consideration domain wall motion in an infinite medium under a given value of an external (dc) E. The domain wall velocity, v, depends only on E; thus, v is also constant. Considering domain coalescence, for a uniformly polarized FE sample under E, the KAI model gives $\Delta P(t)$ as

$$\Delta P(t) = 2P_S\left[1 - \exp\left\{-(t/t_0)^n\right\}\right], \quad (1)$$

where t_0 and n are the characteristic switching time and geometric dimension for the domain growth, respectively, [38]. Note that t_0 should be closely related to v. For the two simplest cases, analytical relationships between t_0 and v can be readily obtained. When nuclei of opposite P are generated at a constant rate throughout the switching process (α model), $t_0 \sim 1/v^{(n-1)/n}$ [38]. When all nuclei are generated instantaneously at the beginning of the switching process (β model), $t_0 \sim 1/v$ [38]. The value of n gives an effective dimension of domain growth, D. For the β model, n is the same as D; for instance, if $n = 2$, then $D = 2$, i.e., two-dimensional domain growth [38]. For the α model, $n = D + 1$ [38].

The KAI model has been used to explain P switching behaviors of numerous FE single crystals [85] and thin films [38,66,73,86,87]. Fig. 3 shows a typical example, i.e., t-dependent switched polarization, $\Delta P(t)$, of 100-nm-thick epitaxial $PbZr_{0.4}Ti_{0.6}O_3$ capacitors reported by So et al. [66]. They measured $\Delta P(t)$ using transient switching current measurements. Detailed experimental methods of switching current measurements have been described elsewhere

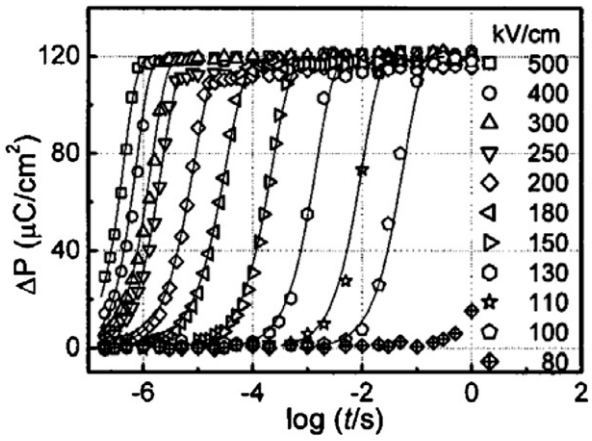

Fig. 3. Time-dependent switched polarization of 100-nm-thick epitaxial $PbZr_{0.4}Ti_{0.6}O_3$ capacitors measured at various electric fields. Solid lines are fitting lines according to the KAI model. Reprinted with permission from [66]. Copyright (2005) by the American Institute of Physics.

[56,66,71]. The KAI model accurately describes the P switching behavior of epitaxial $PbZr_{0.4}Ti_{0.6}O_3$ capacitors (solid fitting lines in Fig. 3) [66]. However, the KAI model assumptions of unrealistic nucleation rates and constant domain wall velocity often limit its applicability to real FE systems.

3.2. Deviation from the KAI model and other approaches

Because the KAI model was formulated for ideal systems, it is not sufficient for describing domain switching kinetics of certain FE materials, particularly those with many quenched defects. Thus, several approaches have been used to explain the discrepancies between the KAI model and real domain switching kinetics by considering finite-size corrections and defects roles such as grain boundaries and defect dipoles. Shur et al. pointed out that a real system is a finite medium, which conflicts with the KAI assumption of an infinite medium [39]. Thus, the KAI model was modified by adding a finite-size correction term, resulting in better agreement with experimental data.

On the other hand, Tagantsev et al. suggested a nucleation-limited-switching (NLS) model to explain the broad switching time distribution observed in polycrystalline films [56]. Domain switching behavior in polycrystalline films proceeds much more slowly than the KAI model predictions. In the prediction of the KAI model, the greatest $\Delta P(t)$ change occurs rather drastically in a one–two-decade time interval (Fig. 3). However, in polycrystalline films, the change in $\Delta P(t)$ occurs progressively over a broad time interval of nearly eight decades (Fig. 4) [56]. The NLS model assumes that films are an ensemble of elementary regions, such as grains, and the domain switching of an individual elementary region is governed by the nucleation process in that region. The local nucleation time varies exponentially, and $\Delta P(t)$ in the NLS model is

$$\Delta P(t) = 2P_S \int_{-\infty}^{\infty} [1 - \exp\{-(t/t_0)^n\}] F(\log t_0) d(\log t_0), \qquad (2)$$

where $F(\log t_0)$ is a distribution function for local switching times [56]. The NLS model explains the broad switching time behavior in polycrystalline films [56,79], indicating that the microstructures, such as grains and their boundaries, significantly affect the switching behavior of FE domains.

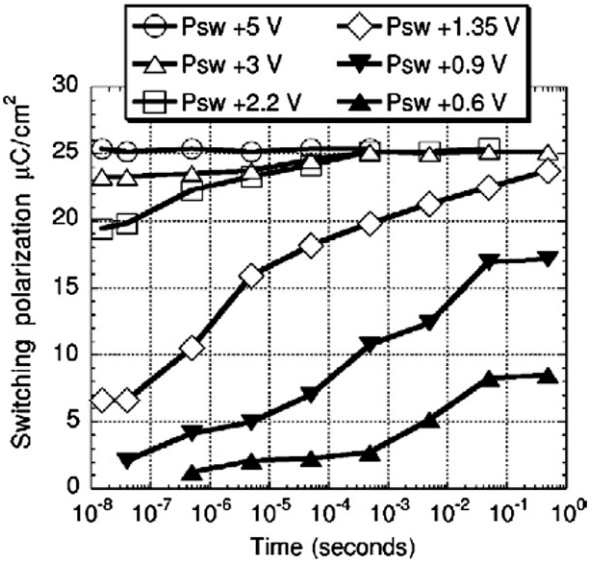

Fig. 4. Time-dependent switched polarization of (111)-oriented 135-nm-thick $PbZr_{0.4}Ti_{0.6}O_3$ films containing Ca, Sr, and La dopants. Reprinted with permission from [56]. Copyright (2002) by the American Physical Society.

Recently, Jo et al. used an advanced approach to investigate the role of defect dipoles on FE domain switching kinetics [71,72]. They investigated the domain switching kinetics of 150-nm-thick (111)-preferred polycrystalline $PbZr_{0.3}Ti_{0.7}O_3$ capacitors over a wide range of E and T [71]. They found that the KAI model predictions deviated markedly from the experimental data in the last switching stage at all measured E and T. Additionally, the best-fitting results with the KAI model gave unreasonable values of n, which were much less than 1 in low E-field regions at all measured values of T (Fig. 5a) [71]. As described in Section 3.1, n indicates the effective dimension of domain growth; therefore, n should be greater than 1. To account for these discrepancies, Jo et al. suggested using the Lorentzian distribution of $\log t_0$ in Eq. (2). As shown in Fig. 5b [71], the fitting result based on the Lorentzian function explains the experimental data quite well, whereas that based on the delta function, i.e., the classical KAI model, does not. Jo et al. suggested that the Lorentzian distribution of $\log t_0$ can be attributed to the local field variation originating from defect dipoles at domain pinning sites.

4. PFM-based experimental studies on nanoscale domain dynamics

4.1. Studies using conventional PFM

In this section, we focus on PFM-based experimental methods, which provide important microscopic details on nucleation and

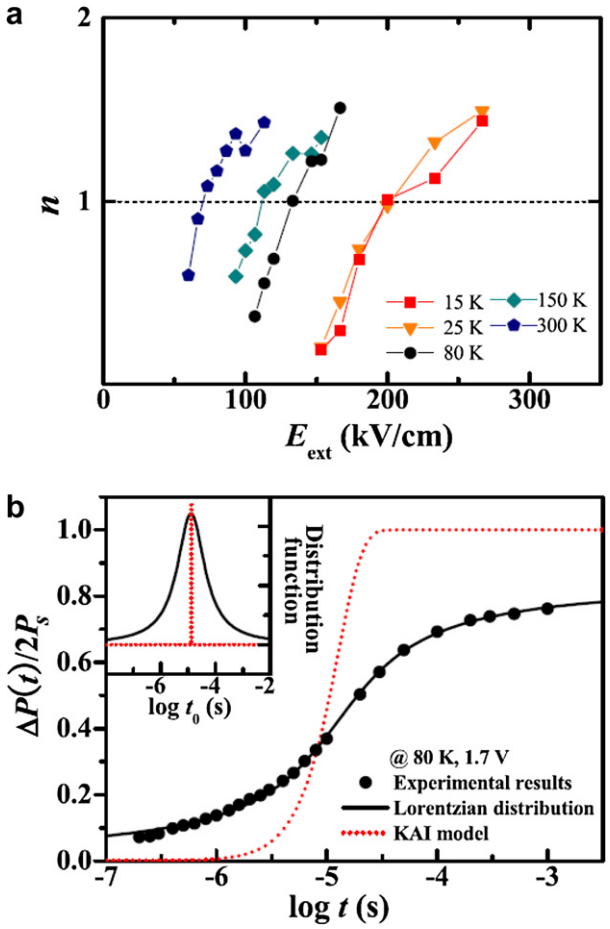

Fig. 5. (a) Values of n for various temperatures and external E. (b) $\Delta P(t)/2P_S$ results for experimental data (solid symbols) and fitting results using the Lorentzian (solid line) and delta (dotted line) distributions for $\log t_0$. The inset shows distribution functions corresponding to the fitted results. Reprinted with permission from [71]. Copyright (2007) by the American Physical Society.

growth of FE domains and demonstrate the relevance of numerical models of domain switching kinetics described in the previous section. PFM, a specialized atomic force microscopy technique, is a powerful method for direct visualization of FE static domain patterns [40–42]. All FEs should exhibit the piezoelectric effect, a linear coupling between mechanical strains and electric fields. PFM detects the converse piezoelectric response of FE materials induced by an applied external ac field. In conventional PFM, an ac bias, $V_{tip} = V_0 \cos \omega t$, is applied to a conductive tip in contact with a bare surface of the sample, i.e., no top electrode (Fig. 6a). It should be noted that the amplitude of V_0 should be smaller than the coercive voltage. The applied ac field induces a local mechanical displacement, $s = s_0 \cos(\omega t + \Phi)$. Here, the amplitude s_0 and phase difference, Φ, indicate the magnitude and direction of P in FE domains, respectively. Using the dual lock-in technique, s_0 and Φ can be measured simultaneously. Details of conventional PFM have been published elsewhere [40–45]. Conventional PFM has been used extensively to study static properties of FE domains [40–45].

FE domain dynamics have not been investigated by conventional PFM as extensively as domain static properties have [40–45,65,88–94]. As shown in Fig. 6a, the applied external E in conventional PFM is highly localized. Thus, domain switching is initiated from a single domain nucleated just below the tip and expands approximately circularly (Fig. 7) [92]. By measuring the pulse width dependence of the reversed domain radius, the domain wall velocity, v, can be estimated. In epitaxial thin films and crystals, the domain size, r, typically varies linearly with an applied E ($r \sim E$) and logarithmically with pulse width, i.e., t ($r \sim \ln t$) [93,94]. Recently, Tybell et al. measured v in epitaxial $PbZr_{0.2}Ti_{0.8}O_3$ thin films under a low E-field regime and found that $v \sim \exp(-1/E)^{\mu}$ with $\mu \sim 1$, where μ is a dynamical exponent related to defect nature [65]. This indicated that FE domain wall motion follows the creep process due to glassy characteristics of randomly pinned domain walls in a disordered system. We discuss the concept of statistical physics in detail in Section 6.

Although the conventional PFM approach is convenient for high spatial resolution, it has several drawbacks for investigating domain wall motion inside real FE devices. First, the applied E is strongly dependent on the tip conditions, such as tip shape, tip radius, and the relative distance between the tip and film, which are often difficult to control. Second, the applied E is not uniform;

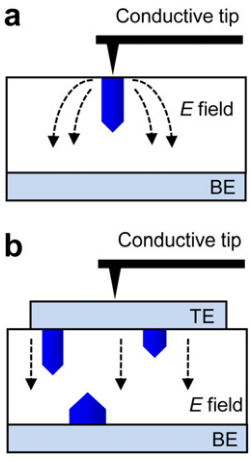

Fig. 6. Sketch of domain nucleation (a) in conventional piezoresponse force microscopy (PFM) and (b) in PFM of the ferroelectric capacitor structure. The dashed arrows indicate the electric field lines. The solid (blue) needle-like figures show reversed nuclei. TE and BE are the top electrode and bottom electrode, respectively. (For interpretation of the references to colour in this figure, the reader is referred to the web version of this article).

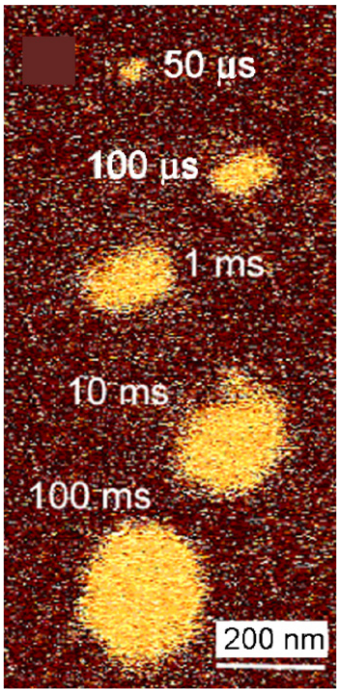

Fig. 7. PFM phase image of domain propagation in a 100-nm-thick epitaxial $PbZr_{0.4}Ti_{0.6}O_3$ film with various pulse widths. Reprinted with permission from [92]. Copyright (2005) by the Korean Physical Society.

thus, complicated analysis is required to estimate accurate E values. Third, conventional PFM can only observe local switching originating from the nucleus just below the tip. However, most FE devices have capacitor geometry, and domain switching originates from numerous nuclei under a uniform external E.

4.2. PFM imaging in FE capacitor geometry

To overcome the limitations of conventional PFM, direct PFM imaging in capacitor geometry has been used [44,45,79,95,96]. In this technique, the entire volume beneath the top electrode is electrically excited, but the piezoresponse is still probed locally when the top electrode is reasonably thin. Thus, direct PFM imaging can provide spatially resolved information on domain structure beneath the top electrode. Uniform E can be applied in this setup to observe the domain switching behavior in real FE devices (Fig. 6b). Thus, in addition to sideways domain motion, it is possible to investigate the nucleation process occurring in real FE devices. Additionally, the effect of the tip on PFM imaging can be reduced. However, direct PFM imaging has slightly lower spatial resolution than conventional PFM. Note that the spatial resolution of direct PFM imaging also depends on the thickness of the FE layer and top electrode. Typically, the resolution is expected to be $\sim 0.2 d_{top}$, where d_{top} is the thickness of the top electrode [97].

Recently, a modified-PFM technique combined with switching current measurements was developed [58,80,98]. Despite several advantages of PFM in capacitor geometry, it is difficult to apply reliable and sufficient E to capacitors with large top electrodes via a conductive tip. The contact between the conductive tip and the top electrode is less stable, because the tip needs to move continuously on the top electrode surface for imaging and tip radius is quite small. To guarantee reliable electric contact, Kim et al. adopted a separate probe needle, schematically depicted in Fig. 8 [58]. Fig. 9 shows a top-view image of the cantilever, probe needle, and capacitor configuration, obtained using an optical

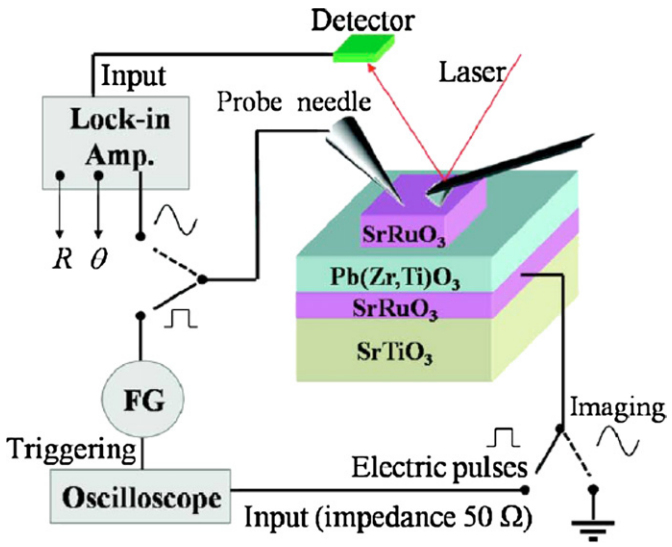

Fig. 8. Schematic of the modified-PFM setup. Reprinted with permission from [58]. Copyright (2007) by the American Institute of Physics.

microscope [98]. The separate probe needle is used to apply an external E (i.e., rectangular pulses for domain switching) and ac modulation field for imaging through a top electrode. With this setup, it is possible to use a nonconductive tip for scanning; thus, additional electrostatic effects can be removed.

Furthermore, by using a separate probe needle, it is possible to perform separate switching current measurement using the PFM setup. The reliability of $\Delta P(t)$ data from PFM can be accessed by comparing the volume of reversed domains from PFM images with ΔP from switching current measurements [58,80,99,100]. Note that, like all scanning probe microscopy techniques, the scanning time for PFM typically takes a few minutes; many FE films may be affected by imprints and relaxation during a scan, decreasing the reliability of the data [10,11,101]. Therefore, a comparison of $\Delta P(t)$ data from both PFM and switching current measurements is essential to verify PFM image reliability.

4.3. Interrupted-switching PFM

Recently developed interrupted-switching PFM techniques are effective for investigating domain switching dynamics in real FE capacitors, as described in Section 2.4. Two primary modifications of the interrupted-switching PFM method have been suggested:

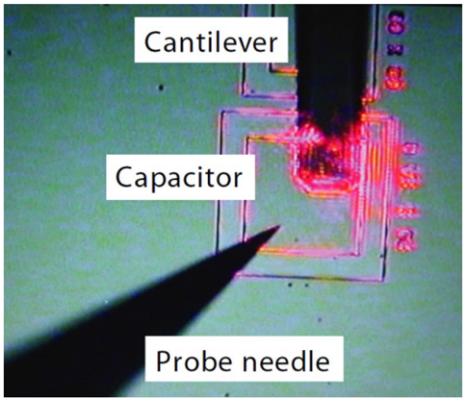

Fig. 9. Top view of the cantilever, probe needle, and capacitor configuration obtained using an optical microscope. Capacitor size in the figure is $100 \times 100\ \mu m^2$. Reprinted with permission from [98]. Copyright (2010) by the Institute of Physics.

the stroboscopic method by Gruverman et al. [79] and the domain-tracing method by Yang et al. [80].

The stroboscopic method applies a series of short input pulses with fixed amplitude and incrementally increasing duration (Fig. 10a) [80]. After each pulse, PFM imaging of the resulting domain pattern is performed. At the beginning of each switching cycle, the capacitor is reset to the initial polarization state. Applicability of this method depends on the reproducibility of domain switching kinetics from cycle to cycle. Because inhomogeneous nucleation occurs in real FE capacitors, this approach is applicable to many FE capacitors [58,79,98,99,102].

However, it is difficult to obtain consecutive PFM images of domain wall evolution during a single P switching process using the stroboscopic method. Note that each poling pulse resets the capacitor at the beginning of each switching cycle in the stroboscopic method. Consequently, even if switching pulses with the same pulse width are used, (i.e., $t_1 = t_2$ in Fig. 10a), the PFM images will be somewhat different due to the stochastic nature of inhomogeneous nucleation. To overcome this drawback, the domain-tracing method uses the pulse sequence shown in Fig. 10b [80]. It applies one poling pulse and then a series of pulses (usually the same pulse width), with PFM imaging between the pulses. It is assumed that the PFM image obtained after the ith pulse is nearly the same as that obtained after a single pulse of $t = \tau_1 + \tau_2 + \ldots + \tau_i$. Thus, all PFM images taken before the $(i+1)$th pulse should reveal the domain wall evolution due to P switching during a single pulse of t, allowing the dynamics of a particular domain to be traced and studied. Several studies on FE domain dynamics have used this method [63,80,100,103]. It should be noted that both variations of the interrupted-switching PFM method rely on the stability of instantaneous domain patterns between pulse applications. As mentioned previously, transient switching current measurements should be used to access the reliability of PFM images and determine whether P relaxation, imprints, and so on, have occurred.

5. Nanoscale PFM studies of defect-mediated FE domain switching dynamics

5.1. Nucleation process

Kim et al. used the modified-PFM technique to investigate microscopic information on the domain nucleation process.

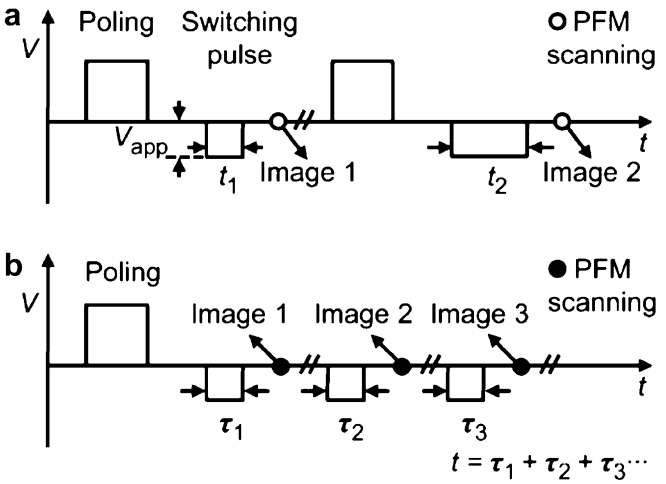

Fig. 10. Schematic of pulse sequences used (a) to employ the stroboscopic-switching approach and (b) the domain-tracing approach. Reprinted with permission from [80]. Copyright (2008) by the American Institute of Physics.

Although defect-mediated nucleation was thought to occur inhomogeneously, as described in Section 2.2, few experimental studies have examined to visualize inhomogeneous nucleation. Kim et al. demonstrated that inhomogeneous nucleation actually occurs in 170-nm-thick $PbZr_{0.4}Ti_{0.6}O_3$ epitaxial films using modified-PFM [58]. Fig. 11a shows the spatial probability distribution of nucleation sites in capacitors obtained by summing 30 phase images [58]. Darker spots indicate positions where nucleation occurred more frequently, and the white area indicates the region where no P reversal occurred during 30 repetitions. Note that if homogeneous nucleation occurs, the nucleation should occur randomly by thermal activation. However, Fig. 11a shows that the nucleation occurred at particular sites. Fig. 11b shows the number of sites for a given probability among the 30 repetitions, indicating that the nucleation probability was very high at the particular sites where nucleation occurred [58]. These experimental results provided direct evidence that inhomogeneous nucleation occurs in FE thin films. They also showed that the nucleation sites changed depending on the bias polarity (Fig. 12) [58]. This polarity dependence of nucleation sites suggests that nucleation is very likely to occur at the FE/electrode interface rather than in the film interior.

Jesse et al. investigated the spatial and energy distributions of nucleation centers in epitaxial $PbZr_{0.2}Ti_{0.8}O_3$ films using conventional PFM geometry [62]. They found that 90° domain wall boundaries and intersections play an important role as nucleation centers, reducing the nucleation energy barrier due to local microstructure or defects.

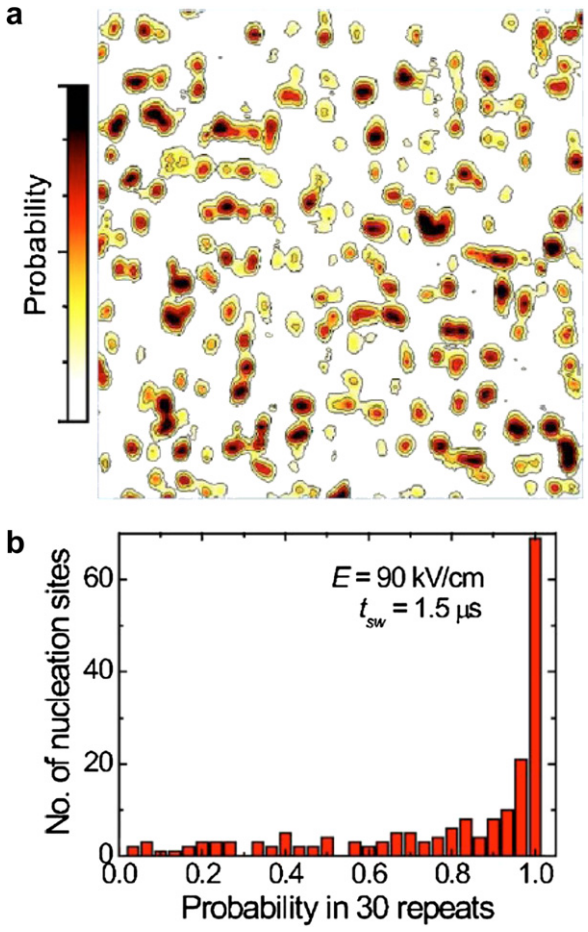

Fig. 11. (a) Spatial probability distribution of nucleation sites in an epitaxial $PbZr_{0.4}Ti_{0.6}O_3$ capacitor. The scan area is $6 \times 6\ \mu m^2$. (b) Numerical distribution of nucleation sites in terms of the probability obtained from (a). Reprinted with permission from [58]. Copyright (2007) by the American Institute of Physics.

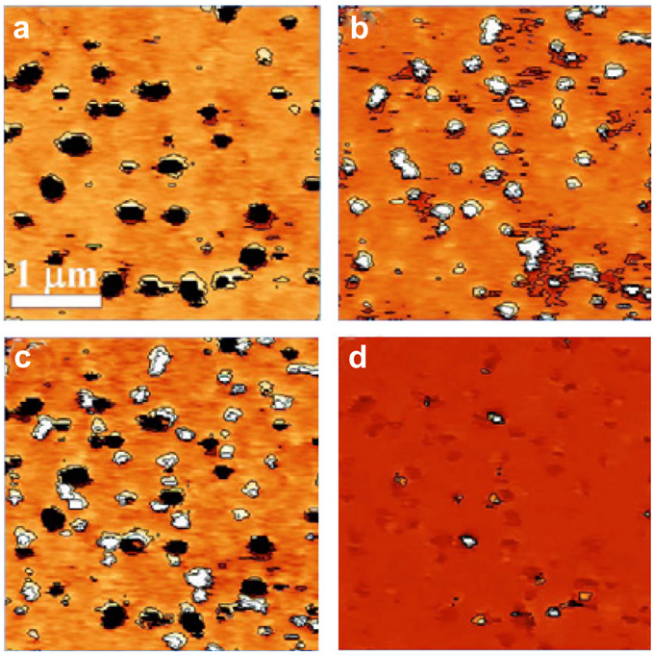

Fig. 12. Visualization of nucleated domains from PFM images under (a) positive ($E = +150$ kV/cm) and (b) negative ($E = -150$ kV/cm) pulses with $t_{sw} = 0.5$ μs. The nucleated domains are shown as dark areas in (a) and as the bright areas in (b). The merged image (c) = (a) + (b) shows that most of the reversed domains under a positive pulse were nucleated at different sites than those under a negative pulse. The difference image (d) = (a) − (b) shows the sites at which reversed domains were nucleated under both positive and negative pulses. Reprinted with permission from [58]. Copyright (2007) by the American Institute of Physics.

These experiments indicate that surfaces and defects play important roles in the domain nucleation process of most FE thin films.

The nucleation process in ultrathin films warrants special attention. Jo et al. suggested that thermodynamic random nucleation is possible in ultrathin films [61]. In FE single domains, a depolarization field is generated by the bound charges at the surface of the FE layer in the direction opposite to P [104,105]. In principle, free charge carriers in the conducting electrodes should compensate for the bound charges. However, the finite screening length of real conducting electrodes results in an incomplete compensation of the P charges. The depolarization field increases with decreasing FE film thickness [104] and causes instable ferroelectricity in FE ultrathin films [6]. Jo et al. showed that large depolarization fields in ultrathin films lowered U_N to a level comparable to thermal energy; thus, nucleation occurred randomly, and P relaxation occurred due to thermal activation [61].

Recently, Highland et al. reported an interesting study on P switching in ultrathin $PbTiO_3$ films using *in situ* synchrotron X-ray scattering. They showed that nucleation was suppressed at high temperatures (near a critical temperature) and occurred by homogeneous switching (referred to in their paper as "continuous mechanism") [52]. In other words, P decreased uniformly and reversed direction without forming domains. They estimated the formation energy of a half-spheroid nucleus as a function of film thickness and temperature based on Landauer's electrostatic consideration [32]. Using this result, they observed that stable nuclei were not formed in ultrathin films near a critical temperature. Although interesting, their results are indirect because the data were obtained from macroscopic measurements. Direct imaging of the nucleation process in ultrathin films capacitors by PFM would be highly interesting. However, direct PFM imaging in ultrathin FE capacitors faces fundamental and technical challenges,

including short time domain relaxation and time resolution of PFM imaging. Nevertheless, improved experimental direct PFM imaging continues to be an active research focus.

5.2. Forward domain growth

It is difficult to investigate direct forward growth of reversed domains in capacitor geometry using PFM. Unlike nucleation and sideways domain wall motion, forward growth occurs along the *c*-direction, as described in Section 2.2. Therefore, uniform *E* throughout the capacitor leads to an averaged piezoelectric response over the film thickness, and data on the depth distribution of *P* are difficult to obtain in capacitor geometry [106].

However, several recent PFM studies investigated forward growth using different sample geometries. Shafer et al. developed planar-electrode PFM [107]. The primary advantage is that the FE film is located between coplanar electrodes, permitting cross-sectional imaging of the FE domain switching process. They investigated the cross-sections of epitaxial 100-nm-thick $BiFeO_3$ capacitors. They showed that a domain of reversed *P* originated in an area near one electrode and progressively grew toward the counter electrode (Fig. 13), similar to the results shown in Fig. 1b and c [107]. This observation indicates that the reversed domain nucleated at the FE/electrode interface and grew across the film. Gysel et al. also prepared columnar structures of rhombohedral and tetragonal (111) $Pb(Zr,Ti)O_3$ capacitors using wafer cleavage followed by polishing with a focused ion beam and carried out cross-sectional PFM imaging [106]. Recently, Balke et al. studied FE domain switching in the in-plane capacitor structure of an epitaxial (110) $BiFeO_3$ film, with geometry similar to planar-electrode PFM [108]. They observed clear forward domain growth as well as nucleation and lateral domain growth and explored the roles of interfacial charge injection and surface screening on switching mechanisms.

5.3. Sideways domain wall motion

PFM is a very powerful method for investigating sideways domain wall motion directly, providing microscopic details on how domain walls propagate in real FE materials with defects. Here, we focus on PFM studies on *t*-dependent sideways domain wall motion in FE thin film capacitor geometry. Nanoscale FE domain studies using the conventional PFM setup have been described elsewhere [37,40–45,64,109].

Gruverman et al. investigated polycrystalline 180-nm-thick (111)-oriented $Pb(Zr,Ti)O_3$ capacitors with $3 \times 3\ \mu m^2$ IrO_2 top electrodes using stroboscopic methods [79]. The step-by-step switching approach allowed direct studies of FE domain switching. They observed that the mechanism of *P* reversal in the polycrystalline capacitors changed during the switching cycle from the initial nucleation-dominated process (in agreement with KAI model fitting) to lateral domain expansion at later stages (in agreement with NLS model fitting). This indicates that the domain switching process in real polycrystalline FE capacitors is quite complicated due to defects, and the role of defects should be considered. Recently, Gruverman et al. studied FE capacitor switching on the order of 10 ns [99]. They observed that small capacitors ($1 \times 1.5\ \mu m^2$ top electrode), in which *P* reversal is dominated by domain wall motion, switched faster at high fields but more slowly at low fields, whereas larger capacitors exhibited the opposite behavior.

Using the domain-tracing method, Yang et al. investigated domain wall motion in 100-nm-thick epitaxial $PbZr_{0.2}Ti_{0.8}O_3$ capacitors with 100 μm diameter top electrodes [80]. Fig. 14 shows successive domain evolution images obtained at the same sample position under different *E* [80]. The reliability of the obtained PFM images was confirmed by separate switching current measurements, as described in Section 4.2. Nucleation was much more important in the early stage of switching and under high voltage, whereas domain wall motion dominated *P* switching under low voltage (Fig. 14). They also observed that domain wall velocity decreased with increasing domain size, consistent with other reports [10,77,110,111].

Recently, interesting studies on directional or anisotropic domain growth in FE capacitors have been reported [103,112]. Kim et al. investigated FE domain wall motion in 200-nm-thick epitaxial (001) $BiFeO_3$ film grown on vicinal (001) $SrTiO_3$ substrate using modified-PFM [103]. They found that directional domain growth depended on the polarity of the applied *E* (Fig. 15a and b) [103]. When a negative voltage was applied through the top electrode, the reversed domain grew along the downhill miscut direction. On the other hand, when a positive voltage was applied, the growth direction was reversed. They explained that the strain gradient due to the vicinal substrate generated a local internal field, breaking the symmetry in the FE double-well potential; the asymmetry resulted in directional domain growth. Wu et al. investigated epitaxial 50-nm-thick (001) $PbZr_{0.2}Ti_{0.8}O_3$ capacitors using the stroboscopic method [112]. They observed that the transition from the low- to high-field range caused a qualitative change in domain growth kinetics: laterally isotropic growth in high fields and highly

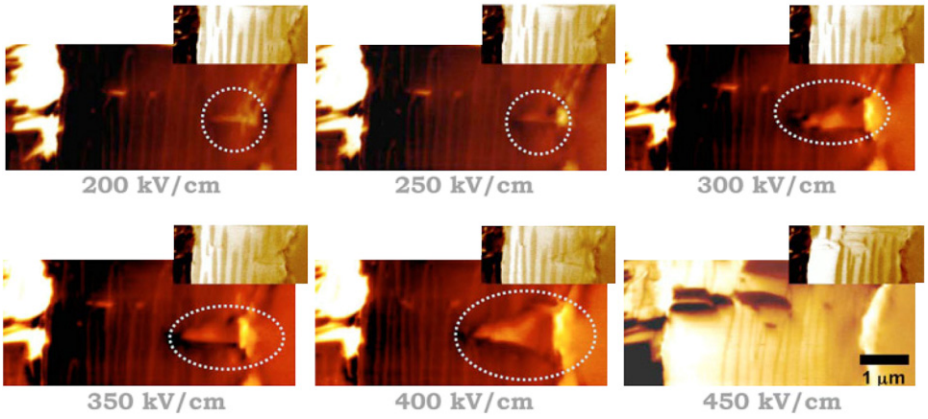

Fig. 13. Growth of a polarization switched region circled from one electrode toward the other as the field strength increased. Small out-of-plane piezoresponse images are set above the larger in-plane piezoresponse images. Reprinted with permission from [107]. Copyright (2007) by the American Institute of Physics.

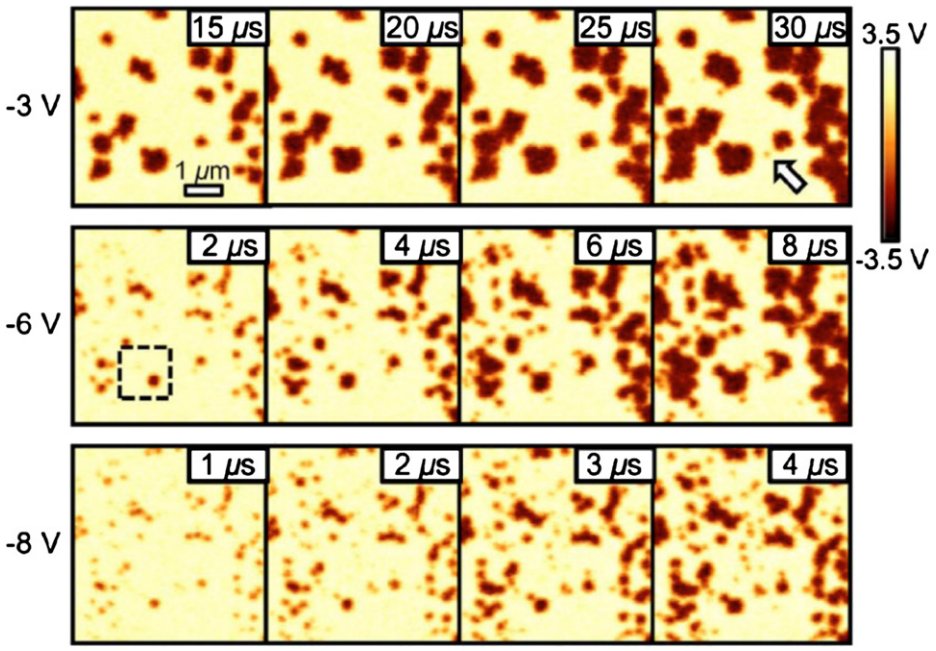

Fig. 14. Visualization of successive domain evolution images obtained at the same sample position under applied voltages of $V_{app} = -3$, -6, and -8 V in an epitaxial $PbZr_{0.2}Ti_{0.8}O_3$ capacitor. The scan area is 5×5 μm^2. Contrast indicates the amount of reversed polarization. Reprinted with permission from [80]. Copyright (2008) by the American Institute of Physics.

anisotropic growth in low fields. These studies demonstrate that nanoscale PFM methods with appropriate time-probing schemes can provide details of FE domain wall motion.

5.4. Discrepancy in the domain wall velocity reported in the literature

These nanoscale studies of sideways domain wall motion highlight the most effective methods for measuring domain wall velocity, v, directly. In the FE community, v is empirically known to be proportional to $\exp(-E_a/E)$, known as the Merz's law [28], where E_a is an activation field. Note that the Merz's law is only valid in the low field regime [2,4] and has the same form as the creep relationship described in Section 4.1 when $\mu = 1$. Fig. 16 shows various literature values of v as a function of $1/E$. The dashed line indicates theoretical v values of bulk $PbTiO_3$, calculated by Shin et al. using multiscale simulations combined with atomistic molecular dynamics and coarse-grained Monte Carlo simulations [113]. The theoretical values provide an upper bound to the wall velocity of real thin films because they do not include the effect of defects. All other data in Fig. 16 are from experiments on $Pb(Zr,Ti)O_3$ (PZT) films at various thicknesses. Solid circles denote the experimental data of Grigoriev et al. measured by X-ray microdiffraction [81]. Solid diamonds and squares represent the modified-PFM data of Kim et al. [98] and Yang et al. [80], respectively. Open symbols indicate the conventional PFM data of Tybell et al. [65]. Although the experimental methods used to measure v and details of film conditions are different, all the data followed the Merz's law, as shown by linear fittings. However, the reported v values decreased with decreasing film thickness. Note that there was large fluctuation among reported values of v and E_a (i.e., the slope of linear fittings). In particular, v at high E varied widely, by orders of 10–11. Few plausible explanations for the discrepancy among experimental v values have been proposed. To understand the source of

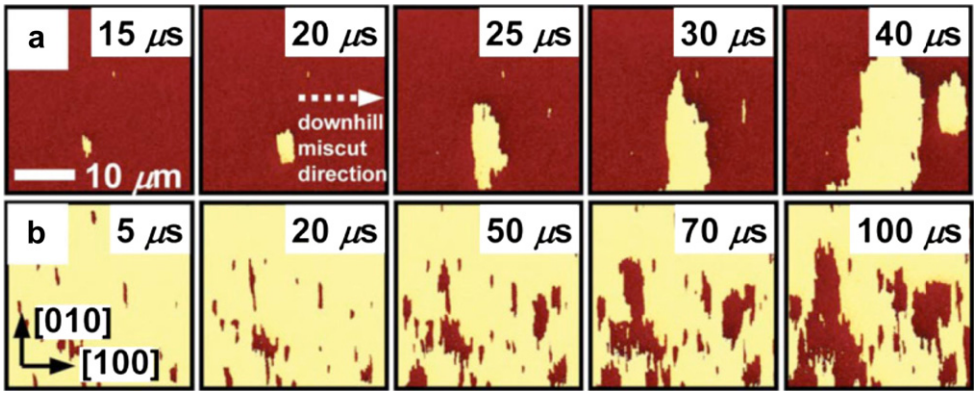

Fig. 15. (a) Out-of-plane PFM phase images of successive FE domain evolution under negative 4.7 V and (b) positive 3.3 V switching voltages after an initial poling process in an epitaxial $BiFeO_3$ capacitor. All PFM phase images were obtained within the same region. The scan size is 30×30 μm^2. Reprinted with permission from [103]. Copyright (2009) by the American Institute of Physics.

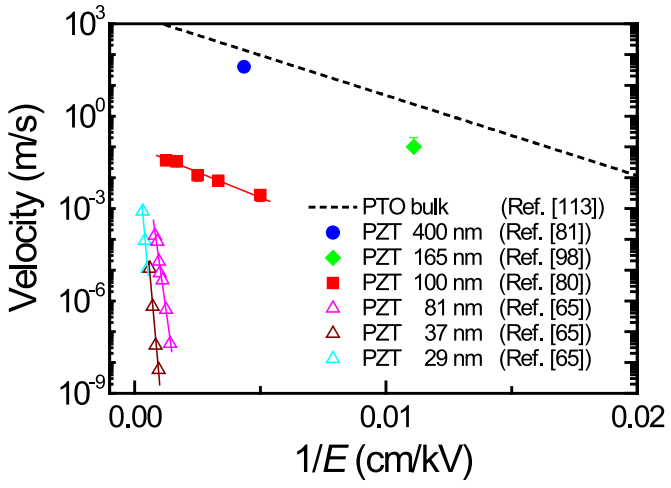

Fig. 16. Domain wall velocities (v) as a function of the inverse external electric field ($1/E$) reported in the literature. (See text for details). The solid linear lines indicate the linear fitting lines based on Merz's law.

the discrepancy, the physics that govern FE domain wall dynamics, largely controlled by defects in FE systems, must be considered.

6. Statistical description of the physics of FE domain wall motion

6.1. Propagation of elastic objects in disordered media

FE domain wall motion is thought of as the propagation of elastic objects in disordered media with quenched defects [63,65,90,91,114]. Propagation of elastic objects in disordered media can explain numerous physical phenomena, including contact lines in wetting, surfaces of epitaxially grown films, vortices in type II superconductors, charge–density waves, dislocation lines, and magnetic domain walls [114–122]. In such media, elastic energy tends to keep elastic objects flat, while the pinning potential of defects locally promotes wandering, as shown schematically in Fig. 17. The dashed (blue) line shows the FE domain wall, and the shape determines the elastic energy. The solid (black) circles indicate quenched defects, generating the pinning potential. Competition between elastic energy and pinning potential leads to a complicated energy landscape with many local minima, which govern the dynamics of elastic objects under a driving force. It is known that the dynamics should undergo continuous pinning–depinning transitions. Near the transition, the depinned domain walls move to the next pinning site; thus, a sequence of discrete and erratic domain jumps, known as a Barkhausen avalanche, can occur [123,124]. Detailed theoretical backgrounds on the physics of elastic objects in disordered media have been published in review papers [114–120], articles [121], and books [122].

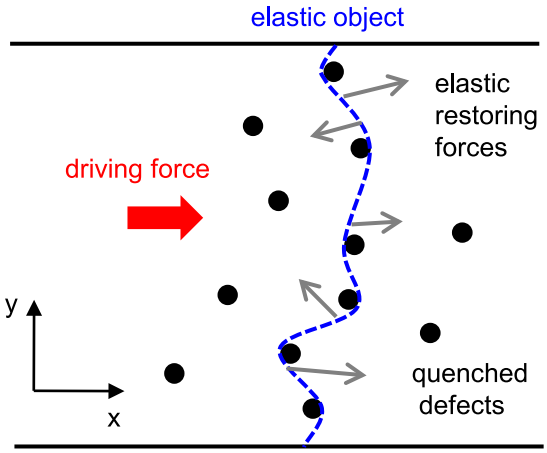

Fig. 17. Schematic of the growth of an elastic object in a disordered medium with quenched defects. The dashed line indicates the elastic object. The solid circles show quenched defects, generating pinning forces. (For interpretation of the references to colour in this figure legend, the reader is referred to the web version of this article).

Fig. 18 shows the t-dependent evolution of domain walls in 170-nm-thick PZT thin films measured by modified-PFM. Note that there are some pinning points where the domain wall cannot move for a certain interval of time. At these pinning sites, local defects probably existed, prohibiting the domain wall from moving freely [125]. After the domain wall was depinned, it moved a certain distance, indicating the occurrence of avalanche-like behavior. Due to the pinning behavior of propagating domain walls, the circular shape of the domain was not maintained [98], and the domain wall became very irregularly shaped. PFM images suggest that continuous pinning–depinning transitions occurred in the FE thin films.

Due to competition between pinning, elastic, and driving forces, v has strongly nonlinear behavior depending on the magnitude of the constant (dc) E. Theoretical predictions of the relationship between v and E are shown in Fig. 19 [63]. At a temperature of $T = 0$, the domain wall remains strongly pinned by local disorders until E reaches a threshold value, E_{C0}, known as the pinned regime, when $v = 0$. When $E \geq E_{C0}$, the domain wall experiences pinning–depinning transition locally and moves with a nonzero velocity, as denoted by the (red) dashed line. This is called the depinning regime,

$$v \sim (E - E_{C0})^{\theta}, \tag{3}$$

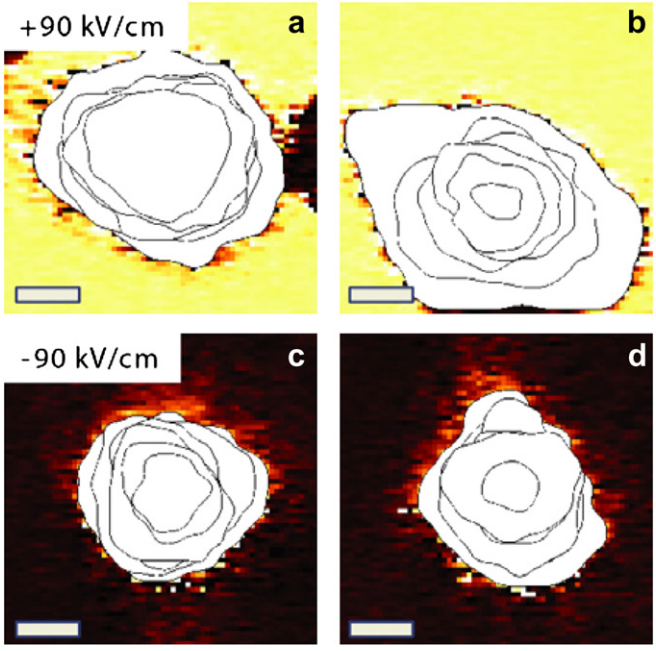

Fig. 18. Overlapped modified-PFM phase images of stepwise-growing domains in 170-nm-thick $PbZr_{0.4}Ti_{0.6}O_3$ thin films. (a) and (b) are at $E = -90$ kV/cm and switching times of $t_{sw} = 316$ ns, 398 ns, 500 ns, 631 ns, 794 ns, and 1.00 μs (from inside to outside); (c) is at $E = 90$ kV/cm and $t_{sw} = 1.00$ μs, 1.26 μs, 1.58 μs, 2.00 μs, 2.51 μs, and 3.16 μs; (d) is at $E = 90$ kV/cm and $t_{sw} = 631$ ns, 798 ns, 1.00 μs, 1.26 μs, 1.58 μs, 2.00 μs, and 2.51 μs. All scale bars are 0.1 μm. Reprinted with permission from [98]. Copyright (2010)by the Institute of Physics.

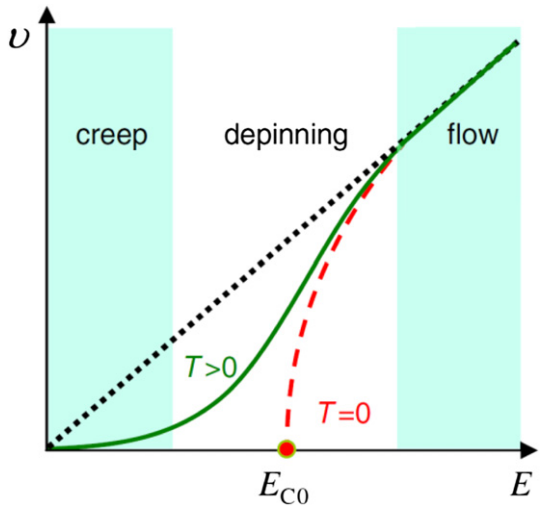

Fig. 19. Theoretical prediction of domain wall velocity, v, vs. electric field, E, in systems governed by competition between disorder and elasticity effects. E_{C0} represents a threshold E. Reprinted with permission from [63]. Copyright (2009) by the American Physical Society. (For interpretation of the references to colour in this figure legend, the reader is referred to the web version of this article).

where θ is a velocity exponent. When $E \gg E_{C0}$, the pinning potential due to quenched defects provides drag force. The domain wall experiences viscous flow motion with $v \sim E$. For a finite T, the dynamic phase transition of second order at $E = E_{C0}$ is smeared, as denoted by the (green) solid line. In this case, under low E (i.e., $E \ll E_{C0}$), thermally activated hopping induces domain wall movement from one local minimum to the next in the so-called creep regime. Then,

$$v \sim \exp\left[-(U/k_B T)(E_{C0}/E)^{\mu}\right], \quad (4)$$

where U is an energy barrier, and μ is a dynamical exponent. Critical exponents of nonlinear domain wall dynamics, including μ and θ, can identify the universality class and provide information on pinning forces and the fractal nature of rough FE domain walls [63,122]. Note that v exhibits strong T-dependence in the creep regime, whereas v is nearly T-independent in the flow regime (Fig. 19).

6.2. Experimental studies on nonlinear dc dynamics of FE domain walls

Recently, there have been remarkable experimental studies to investigate nonlinear FE domain wall dynamics. As described in Section 4.1, Tybell et al. investigated thermally activated creep motion in epitaxial $PbZr_{0.2}Ti_{0.8}O_3$ thin films using conventional PFM [65]. They observed that $\mu \sim 1$, indicating a long-range pinning potential due to defect nature, i.e., random field type. Later, Paruch et al. studied creep motion in an epitaxial $PbZr_{0.2}Ti_{0.8}O_3$ thin film by measuring the roughness exponent, ζ, of the static domain wall configuration [90,91]. They determined that $\zeta \sim 0.26$, indicating an effective domain wall dimensionality of $D \sim 2.5$ [90]. Despite this pioneering work, only the creep regime was investigated, i.e., low E field. Additionally, Bonnell et al. noted that reliable measurements of field-dependent domain wall dynamics in tip-induced switching are extremely difficult to obtain due to nonuniform E of the conductive tip in conventional PFM [44].

Recently, Jo et al. investigated the dc field-driven domain wall dynamics of epitaxial PZT films under wide T and E ranges [63]. They showed that the entire dc field-driven domain wall dynamics, including creep, depinning, and flow motion, occurred in the FE system. Fig. 20 shows v vs. E data [63], similar to the theoretical

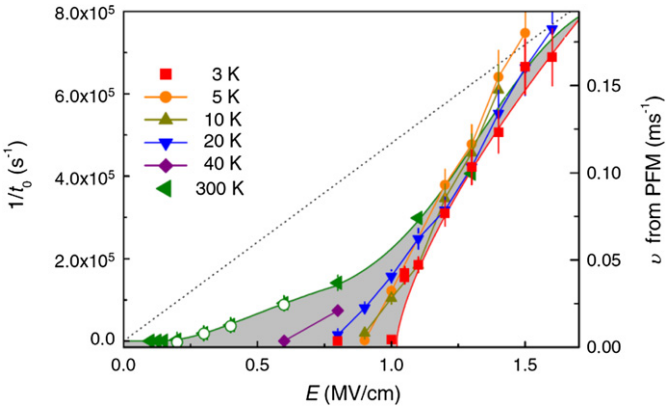

Fig. 20. Temperature-dependent experimental data of $1/t_0$ (solid symbols) vs. E in an epitaxial $PbZr_{0.2}Ti_{0.8}O_3$ capacitor. Open circles indicate the v data from PFM. Reprinted with permission from [63]. Copyright (2009) by the American Physical Society.

predictions in Fig. 19. Jo et al. first measured v at room temperature using modified PFM with the domain-tracing method [80]. Then, to widen the accessible region of T and E, they performed switching current measurements at 3–300 K. Using $v \sim 1/t_0$ in the KAI model [38], they obtained v values. Experimental data showed that $\mu \sim 1$, representing the random field disorder of their epitaxial $PbZr_{0.2}Ti_{0.8}O_3$ capacitors [63]. They also determined that $\theta \sim 0.7$, giving the fractal dimension of FE domain walls, $D \sim 1.4$ [63]. This D value is consistent with recent reports on the fractal dimension of static domain walls in FE thin films [126,127].

Yang et al. recently extended this study of nonlinear dc dynamics to ac domain dynamics in epitaxial $PbZr_{0.2}Ti_{0.8}O_3$ capacitors [70]. Similar studies have been performed for magnetic domain walls [128–130] but not for FE domain walls. Yang et al. showed that the frequency dependence of P–E hysteresis loops can be understood in terms of the ac dynamics of elastic objects in disordered media. They discovered that, depending on the measurement frequency, a dynamic crossover between the creep and flow regimes can occur. This dynamic crossover determines the shape of the P–E hysteresis loop, similar to ferromagnetic systems [128,129].

7. Remaining issues and perspectives

Recently, numerous investigations have explored the propagation of magnetic domain walls because it is an important issue in condensed matter physics [131–135]. Although much effort has been focused on understanding magnetic domain walls (using nonlinear dynamics of elastic objects in disordered media, in

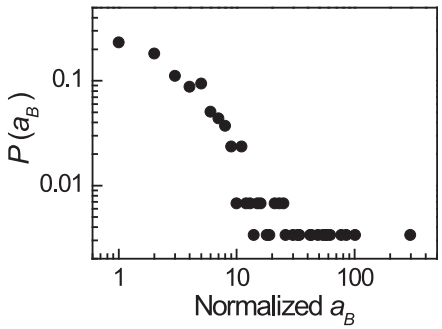

Fig. 21. Size distribution of the Barkhausen avalanche (a_B). Normalized a_B values were obtained by dividing by the unit pixel size. $P(a_B)$ indicates the normalized relative probability of a_B.

particular), little effort has been focused on FE domain walls. Therefore, studies on defect-mediated domain switching dynamics in real FE materials are important.

Currently, several important issues of general interest remain. First, systematic studies of *T*-dependent PFM imaging on FE domain dynamics should be performed. FE materials depend strongly on *T*, such as the critical Curie temperature and structural transition temperature. Additionally, nucleation and domain wall motion involve thermally activated processes [2–4]. Therefore, *T*-dependent PFM imaging can provide new information on the fundamental mechanism of FE domain switching. One example of potential studies is an investigation of the FE domain switching mechanism in ultrathin films at high *T*. As mentioned in Section 5.1, Highland et al. recently reported that continuous *P* switching occurs in ultrathin films at high *T* [52]. To probe this intriguing phenomenon using PFM, the *P* switching behavior should be probed near the Curie temperature. Additionally, as described in Section 6.2, efforts to directly measure the domain wall velocity of growing domains using PFM under a wide range of *T* can elucidate nonlinear domain wall dynamics.

Second, refined values of the fractal dimension of domain growth, the correlation length exponent, and many other important quantities should be obtained using nanoscale imaging with enhanced spatial resolution. According to the scaling theory of elastic interface propagation in media with defects, five scaling exponents characterize the universality class of the system: roughness, growth, dynamics, velocity, and correlation length [122]. Such exponents should be related to one another by scaling relationships [122]. Recent nanoscale studies addressed these points and measured some exponents experimentally [63,90], but most exponents are still unknown. It is important to determine the universality class of numerous FE systems to reveal the nature of the fundamental interactions. Additionally, values from FE systems could be compared with reported values from magnetic systems. Thus, future efforts should focus on measuring scaling exponents in numerous FE systems.

There is also interest in visualization of Barkhausen avalanches in FE systems. The Barkhausen avalanche, a self-organized criticality phenomenon [136], is a paradigm in physics used to explain many natural phenomena such as earthquakes, fluids invading fronts, and even fluctuation in the stock market [137]. Because FE materials also have many pinning sites for propagation of domain walls and undergo continuous pinning–depinning transitions, Barkhausen jumps should occur during FE domain wall motion, similar to other ferromagnetic systems [124,137–140]. Some reports have investigated FE fields by electrical measurements [141]; however, there are no reports of direct visualization. Fig. 21 shows the size distribution for areas of Barkhausen avalanches (a_B) in 200-nm-thick epitaxial $BiFeO_3$ (001) thin film capacitors, which were measured recently using modified PFM. Barkhausen avalanches in FE systems were confirmed by a power law relationship between a_B and normalized relative probabilities of a_B, namely $P(a_B)$, i.e., $P(a_B) \sim {a_B}^{-\tau}$, where τ is a critical exponent. It is difficult to clearly observe the power law relationship in Fig. 21, because the data are not sufficient, especially in smaller a_B regions. Additionally, there are other obstacles, such as spatial resolution and discrete imaging limitations in interrupted-PFM methods. Solutions for such obstacles will enable systematic studies of the Barkhausen avalanche in FE domain wall motion.

In technical point of view, it should be highly required to enhance spatial resolution of PFM imaging, scanning time, piezoresponse sensitivity, and other parameters for detailed analyses. Much effort has been focused on developing enhanced PFM techniques. One example is a modified-PFM setup for applying a reliable electric field and carrying out simultaneous transient switching current measurements [58,80]. Other examples include high-speed PFM by Huey's group, which increased time resolution by two orders of magnitude compared with conventional PFM imaging [142,143], and resonance-enhanced PFM by Jesse et al., which enabled imaging of weakly piezoelectric materials and probing of inelastic phenomena in FE materials [144]. Recently, Rodriguez et al. demonstrated high-resolution PFM imaging in a liquid environment [145]. Despite such efforts, a versatile imaging tool for FE domain switching dynamics has not been developed. Advancements in nanoscale dynamics investigation tools should facilitate scientific efforts for a fundamental understanding of nanoscale FE domain switching dynamics.

8. Conclusion

FE domain switching dynamics should be investigated on the nanoscale to promote applications of FE materials in multifunctional smart electronic devices. Recently, multiferroic materials, which have more than two ferroic orders in the same material, have increased the awareness of FE materials and their domain switching dynamics. PFM can provide unique opportunities for studying the physical mechanisms responsible for the dynamic properties of FE domains at the nanoscale. Recent developments in interrupted-switching PFM approaches and modified-PFM methods have enabled investigations of defect-mediated FE domain dynamics in thin film capacitors with both nanoscale spatial and time resolution. New experimental efforts using PFM-based methods have provided insight into the fundamental physics underlying FE domain wall motion, i.e., the dynamics of elastic objects in disordered media. A fundamental understanding of FE domain switching dynamics will facilitate engineered domains for smart FE device applications.

Acknowledgement

We appreciate careful reading of this manuscript by T. H. Kim. This work was supported by the National Research Foundation of Korea (NRF) grant funded by the Ministry of Education, Science and Technology (MEST) (Grants No. 2009-0080567 and No. 2010-0020416). J.-G. Yoon acknowledges support from Basic Science Research Program through the NRF funded by the MEST (No. 2010-0008341).

References

[1] J. Valasek, Phys. Rev. 15 (1920) 537.
[2] E. Fatuzzo, W.J. Merz, Ferroelectricity. North-Holland Publishing Co., Amsterdam, 1967.
[3] M.E. Lines, A.M. Glass, Principles and Applications of Ferroelectrics and Related Materials. Clarendon Press, Oxford, 1977.
[4] G.A. Smolenskii, Ferroelectrics and Related Materials. Gordon and Breach Science Publisher, Amsterdam, 1984.
[5] R.E. Cohen, Nature 358 (1992) 136.
[6] J. Junquera, P. Ghosez, Nature 422 (2003) 506.
[7] D.D. Fong, G.B. Stephenson, S.K. Streiffer, J.A. Eastman, O. Auciello, P.H. Fuoss, C. Thompson, Science 304 (2004) 1650.
[8] J.H. Haeni, P. Irvin, W. Chang, R. Uecker, P. Reiche, Y.L. Li, S. Choudhury, W. Tian, M.E. Hawley, B. Craigo, A.K. Tagantsev, X.Q. Pan, S.K. Streiffer, L.Q. Chen, S.W. Kirchoefer, J. Levy, D.G. Schlom, Nature 430 (2004) 758.
[9] B.H. Park, B.S. Kang, S.D. Bu, T.W. Noh, J. Lee, W. Jo, Nature 401 (1999) 682.
[10] J.F. Scott, Ferroelectric Memories. Springer, Berlin, 2000.
[11] M. Dawber, K.M. Rabe, J.F. Scott, Rev. Mod. Phys. 77 (2005) 1083.
[12] N. Setter, D. Damjanovic, L. Eng, G. Fox, S. Gevorgian, S. Hong, A. Kingon, H. Kohlstedt, N.Y. Park, G.B. Stephenson, I. Stolitchnov, A.K. Taganstev, D.V. Taylor, T. Yamada, S. Streiffer, J. Appl. Phys. 100 (2006).
[13] J.F. Scott, J. Phys.: Condens. Matter. 18 (2006) R361.
[14] K.J. Choi, M. Biegalski, Y.L. Li, A. Sharan, J. Schubert, R. Uecker, P. Reiche, Y.B. Chen, X.Q. Pan, V. Gopalan, L.Q. Chen, D.G. Schlom, C.B. Eom, Science 306 (2004) 1005.
[15] C.H. Ahn, K.M. Rabe, J.M. Triscone, Science 303 (2004) 488.
[16] K.M. Rabe, C.H. Ahn, J.-M. Triscone, Physics of Ferroelectrics: A Modern Perspective. Springer, Berlin, 2007.

[17] J.F. Scott, Science 315 (2007) 954.
[18] S. Mathews, R. Ramesh, T. Venkatesan, J. Benedetto, Science 276 (1997) 238.
[19] H.N. Lee, D. Hesse, N. Zakharov, U. Gösele, Science 296 (2002) 2006.
[20] V. Nagarajan, A. Roytburd, A. Stanishevsky, S. Prasertchoung, T. Zhao, L. Chen, J. Melngailis, O. Auciello, R. Ramesh, Nat. Mater. 2 (2003) 43.
[21] M. Stengel, N.A. Spaldin, Nature 443 (2006) 679.
[22] H.N. Lee, H.M. Christen, M.F. Chisholm, C.M. Rouleau, D.H. Lowndes, Nature 433 (2005) 395.
[23] V.L. Ginzburg, Zh. Eksp. Teor. Fiz. 19 (1949) 36.
[24] A.F. Devonshire, Phi. Mag. 40 (1949) 1040.
[25] L.D. Landau, Phys. Z. Sowjetunion. 11 (1937) 26.
[26] Y.S. Kim, D.H. Kim, J.D. Kim, Y.J. Chang, T.W. Noh, J.H. Kong, K. Char, Y.D. Park, S.D. Bu, J.G. Yoon, J.S. Chung, Appl. Phys. Lett. 86 (2005) 102907.
[27] T. Tybell, C.H. Ahn, J.M. Triscone, Appl. Phys. Lett. 75 (1999) 856.
[28] W.J. Merz, Phys. Rev. 95 (1954) 690.
[29] W.J. Merz, J. Appl. Phys. 27 (1956) 938.
[30] R.C. Miller, G. Weinreich, Phys. Rev. 117 (1960) 1460.
[31] R. Landauer, D.R. Young, M.E. Drougard, J. Appl. Phys. 27 (1956) 752.
[32] R. Landauer, J. Appl. Phys. 28 (1957) 227.
[33] J.A. Hooton, W.J. Merz, Phys. Rev. 98 (1955) 409.
[34] H.L. Stadler, P.J. Zachmanidis, J. Appl. Phys. 34 (1963) 3255.
[35] Y. Luo, I. Szafraniak, N.D. Zakharov, V. Nagarajan, M. Steinhart, R.B. Wehrspohn, J.H. Wendorff, R. Ramesh, M. Alexe, Appl. Phys. Lett. 83 (2003) 440.
[36] J. Kim, S.A. Yang, Y.C. Choi, J.K. Han, K.O. Jeong, Y.J. Yun, D.J. Kim, S.M. Yang, D. Yoon, H. Cheong, K.S. Chang, T.W. Noh, S.D. Bu, Nano Lett. 8 (2008) 1813.
[37] A. Gruverman, A. Kholkin, Rep. Prog. Phys. 69 (2006) 2443.
[38] Y. Ishibashi, Y. Takagi, J. Phys. Soc. Jpn. 31 (1971) 506.
[39] V. Shur, E. Rumyantsev, S. Makarov, J. Appl. Phys. 84 (1998) 445.
[40] A. Gruverman, O. Auciello, H. Tokumoto, Annu. Rev. Mater. Sci. 28 (1998) 101.
[41] S. Hong, J. Woo, H. Shin, J.U. Jeon, Y.E. Pak, E.L. Colla, N. Setter, E. Kim, K. No, J. Appl. Phys. 89 (2001) 1377.
[42] M. Alexe, A. Gruverman, Ferroelectrics at Nanoscale: Scanning Probe Microscopy Approach. Springer, New York, 2004.
[43] S.V. Kalinin, A. Rar, S. Jesse, IEEE. Trans. Ultrason. Ferroelectr. Freq. Control. 53 (2006) 2226.
[44] D.A. Bonnell, S.V. Kalinin, A.L. Kholkin, A. Gruverman, MRS. Bull. 34 (2009) 648.
[45] A. Gruverman, J. Mater. Sci. 44 (2009) 5182.
[46] S. Ducharme, V.M. Fridkin, A.V. Bune, S.P. Palto, L.M. Blinov, N.N. Petukhova, S.G. Yudin, Phys. Rev. Lett. 84 (2000) 175.
[47] R. Dan, et al., J. Phys.: Condens. Matter. 10 (1998) 477.
[48] M. Sepliarsky, S.R. Phillpot, S.K. Streiffer, M.G. Stachiotti, R.L. Migoni, Appl. Phys. Lett. 79 (2001) 4417.
[49] G. Vizdrik, S. Ducharme, V.M. Fridkin, S.G. Yudin, Phys. Rev. B 68 (2003) 094113.
[50] C. Kittel, Introduction to Solid State Physics, seventh ed. Wiley, New York, 1996.
[51] J.F. Scott, A. Gruverman, D. Wu, I. Vrejoiu, M. Alexe, J. Phys.: Condens. Matter. 20 (2008).
[52] M.J. Highland, T.T. Fister, M.-I. Richard, D.D. Fong, P.H. Fuoss, C. Thompson, J.A. Eastman, S.K. Streiffer, G.B. Stephenson, Phys. Rev. Lett. 105 (2010) 167601.
[53] R.L. Moreira, Phys. Rev. Lett. 88 (2002) 179701.
[54] A.M. Bratkovsky, A.P. Levanyuk, Phys. Rev. Lett. 87 (2001) 019701.
[55] A.M. Bratkovsky, A.P. Levanyuk, Phys. Rev. Lett. 85 (2000) 4614.
[56] A.K. Tagantsev, I. Stolichnov, N. Setter, J.S. Cross, M. Tsukada, Phys. Rev. B 66 (2002) 214109.
[57] G. Gerra, A.K. Tagantsev, N. Setter, Phys. Rev. Lett. 94 (2005) 107602.
[58] D.J. Kim, J.Y. Jo, T.H. Kim, S.M. Yang, B. Chen, Y.S. Kim, T.W. Noh, Appl. Phys. Lett. 91 (2007) 132903.
[59] A.-Q. Jiang, H.J. Lee, C.S. Hwang, T.-A. Tang, Phys. Rev. B 80 (2009) 024119.
[60] A.N. Morozovska, E.A. Eliseev, Y. Li, S.V. Svechnikov, P. Maksymovych, V.Y. Shur, V. Gopalan, L.-Q. Chen, S.V. Kalinin, Phys. Rev. B 80 (2009) 214110.
[61] J.Y. Jo, D.J. Kim, Y.S. Kim, S.B. Choe, T.K. Song, J.G. Yoon, T.W. Noh, Phys. Rev. Lett. 97 (2006) 247602.
[62] S. Jesse, B.J. Rodriguez, S. Choudhury, A.P. Baddorf, I. Vrejoiu, D. Hesse, M. Alexe, E.A. Eliseev, A.N. Morozovska, J. Zhang, L.Q. Chen, S.V. Kalinin, Nat. Mater. 7 (2008) 209.
[63] J.Y. Jo, S.M. Yang, T.H. Kim, H.N. Lee, J.G. Yoon, S. Park, Y. Jo, M.H. Jung, T.W. Noh, Phys. Rev. Lett. 102 (2009) 045701.
[64] S.V. Kalinin, B.J. Rodriguez, A.Y. Borisevich, A.P. Baddorf, N. Balke, H.J. Chang, L.-Q. Chen, S. Choudhury, S. Jesse, P. Maksymovych, M.P. Nikiforov, S.J. Pennycook, Adv. Mater. 22 (2010) 314.
[65] T. Tybell, P. Paruch, T. Giamarchi, J.M. Triscone, Phys. Rev. Lett. 89 (2002) 097601.
[66] Y.W. So, D.J. Kim, T.W. Noh, J.-G. Yoon, T.K. Song, Appl. Phys. Lett. 86 (2005) 092905.
[67] Y. Ishibashi, H. Orihara, Integr. Ferroelectr. 9 (1995) 57.
[68] X. Du, I.W. Chen, Mat. Res. Soc. Proc. 493 (1998) 311.
[69] D.J. Jung, M. Dawber, J.F. Scott, L.J. Sinnamon, J.M. Gregg, Integr. Ferroelectr. 48 (2002) 59.
[70] S.M. Yang, J.Y. Jo, T.H. Kim, J.G. Yoon, T.K. Song, H.N. Lee, Z. Marton, S. Park, Y. Jo, T.W. Noh, Phys. Rev. B 82 (2010) 174125.
[71] J.Y. Jo, H.S. Han, J.G. Yoon, T.K. Song, S.H. Kim, T.W. Noh, Phys. Rev. Lett. 99 (2007) 267602.
[72] J.Y. Jo, S.M. Yang, H.S. Han, D.J. Kim, W.S. Choi, T.W. Noh, T.K. Song, J.G. Yoon, C.Y. Koo, J.H. Cheon, S.H. Kim, Appl. Phys. Lett. 92 (2008) 012917.
[73] T.H. Kim, J.Y. Jo, S.M. Yang, D.H. Kim, S. Park, Y. Jo, J.G. Yoon, T.K. Song, J. Korean Phys. Soc. 56 (2010) 503.
[74] C.-L. Jia, S.-B. Mi, K. Urban, I. Vrejoiu, M. Alexe, D. Hesse, Nat. Mater. 7 (2008) 57.
[75] J. Ricote, R.W. Whatmore, D.J. Barber, J. Phys.: Condens. Matter. 12 (2000) 323.
[76] R. Luthi, H. Haefke, K.P. Meyer, E. Meyer, L. Howald, H.J. Guntherodt, J. Appl. Phys. 74 (1993) 7461.
[77] C.S. Ganpule, A.L. Roytburd, V. Nagarajan, B.K. Hill, S.B. Ogale, E.D. Williams, R. Ramesh, J.F. Scott, Phys. Rev. B 65 (2001) 014101.
[78] J.H. Lee, M.R. Choi, Y.J. Oh, W. Jo, Appl. Phys. Lett. 91 (2007) 072906.
[79] A. Gruverman, B.J. Rodriguez, C. Dehoff, J.D. Waldrep, A.I. Kingon, R.J. Nemanich, J.S. Cross, Appl. Phys. Lett. 87 (2005) 082902.
[80] S.M. Yang, J.Y. Jo, D.J. Kim, H. Sung, T.W. Noh, H.N. Lee, J.G. Yoon, T.K. Song, Appl. Phys. Lett. 92 (2008) 252901.
[81] A. Grigoriev, D.-H. Do, D.M. Kim, C.-B. Eom, B. Adams, E.M. Dufresne, P.G. Evans, Phys. Rev. Lett. 96 (2006) 187601.
[82] P.G. Evans, D.-H. Do, E.D. Isaacs, D.M. Kim, C.B. Eom, A.E.M. Dufresne, Nat. Mater. 3 (2004) 365.
[83] A.N. Kolmogorov, Izv. Akad. Nauk. Ser. Math. 3 (1937) 355.
[84] M. Avrami, J. Chem. Phys. 9 (1941) 177.
[85] T.D. Usher, C.P. Poole, H.A. Farach, Ferroelectrics 110 (1990) 67.
[86] J.F. Scott, L. Kammerdiner, M. Parris, S. Traynor, V. Ottenbacher, A. Shawabkeh, W.F. Oliver, J. Appl. Phys. 64 (1988) 787.
[87] K. Dimmler, M. Parris, D. Butler, S. Eaton, B. Pouligny, J.F. Scott, Y. Ishibashi, J. Appl. Phys. 61 (1987) 5467.
[88] K.S. Song, C.H. Kim, H.B. Moon, S.S. Min, J.H. Cho, J. Korean Phys. Soc. 51 (2007) S143.
[89] Y.H. Jang, Q. Zhang, C.H. Kim, H.J. Hwang, J.H. Cho, S.H. Kim, J. Korean Phys. Soc. 56 (2010) 443.
[90] P. Paruch, T. Giamarchi, J.M. Triscone, Phys. Rev. Lett. 94 (2005) 197601.
[91] P. Paruch, T. Giamarchi, T. Tybell, J.-M. Triscone, J. Appl. Phys. 100 (2006) 051608.
[92] Y.W. So, D.J. Kim, T.W. Noh, J.G. Yoon, T.K. Song, J. Korean Phys. Soc. 46 (2005) 40.
[93] J. Woo, S. Hong, N. Setter, H. Shin, J.-U. Jeon, Y.E. Pak, K. No, J. Vac. Sci. Technol. B19 (2001) 818.
[94] P. Paruch, T. Tybell, J.M. Triscone, Appl. Phys. Lett. 79 (2001) 530.
[95] S. Hong, E.L. Colla, E. Kim, D.V. Taylor, A.K. Tagantsev, P. Muralt, K. No, N. Setter, J. Appl. Phys. 86 (1999) 607.
[96] A. Gruverman, B.J. Rodriguez, A.I. Kingon, R.J. Nemanich, A.K. Tagantsev, J.S. Cross, M. Tsukada, Appl. Phys. Lett. 83 (2003) 728.
[97] S.V. Kalinin, B.J. Rodriguez, S.H. Kim, S.K. Hong, A. Gruverman, E.A. Eliseev, Appl. Phys. Lett. 92 (2008) 152906.
[98] D.J. Kim, J.Y. Jo, Y.S. Kim, T.K. Song, J. Phys. D. Appl. Phys. 43 (2010) 395403.
[99] A. Gruverman, D. Wu, J.F. Scott, Phys. Rev. Lett. 100 (2008) 097601.
[100] S.M. Yang, J.W. Heo, H.N. Lee, T.K. Song, J.G. Yoon, J. Korean Phys. Soc. 55 (2009) 820.
[101] D.J. Kim, J.Y. Jo, Y.S. Kim, Y.J. Chang, J.S. Lee, J.G. Yoon, T.K. Song, T.W. Noh, Phys. Rev. Lett. 95 (2005).
[102] A. Wu, P.M. Vilarinho, D. Wu, A. Gruverman, Appl. Phys. Lett. 93 (2008) 262906.
[103] T.H. Kim, S.H. Baek, S.M. Yang, S.Y. Jang, D. Ortiz, T.K. Song, J.S. Chung, C.B. Eom, T.W. Noh, J.G. Yoon, Appl. Phys. Lett. 95 (2009) 262902.
[104] R.R. Mehta, B.D. Silverman, J.T. Jacobs, J. Appl. Phys. 44 (1973) 3379.
[105] D.J. Kim, J.Y. Jo, Y.S. Kim, Y.J. Chang, J.S. Lee, J.-G. Yoon, T.K. Song, T.W. Noh, Phys. Rev. Lett. 95 (2005) 237602.
[106] R. Gysel, A.K. Tagantsev, I. Stolichnov, N. Setter, M. Pavius, Appl. Phys. Lett. 89 (2006) 082906.
[107] P. Shafer, F. Zavaliche, Y.H. Chu, P.L. Yang, M.P. Cruz, R. Ramesh, Appl. Phys. Lett. 90 (2007) 202909.
[108] N. Balke, M. Gajek, A.K. Tagantsev, L.W. Martin, Y.-H. Chu, R. Ramesh, S.V. Kalinin, Adv. Funct. Mater. 20 (2010) 3466.
[109] P. Maksymovych, S. Jesse, M. Huijben, R. Ramesh, A. Morozovska, S. Choudhury, L.Q. Chen, A.P. Baddorf, S.V. Kalinin, Phys. Rev. Lett. 102 (2009) 4.
[110] T.K. Song, S.M. Yang, J. Korean Phys. Soc. 55 (2009) 618.
[111] A.J. Bray, Adv. Phys. 43 (1994) 357.
[112] D. Wu, I. Vrejoiu, M. Alexe, A. Gruverman, Appl. Phys. Lett. 96 (2010) 112903.
[113] Y.-H. Shin, I. Grinberg, I.W. Chen, A.M. Rappe, Nature 449 (2007) 881.
[114] W. Kleemann, Annu. Rev. Mater. Res. 37 (2007) 415.
[115] P.G. de Gennes, Rev. Mod. Phys. 57 (1985) 827.
[116] L.B. Ioffe, V.M. Vinokur, J. Phys. C: Solid State Phys. 20 (1987) 6149.
[117] G. Gruner, Rev. Mod. Phys. 60 (1988) 1129.
[118] D.S. Fisher, Phys. Rep. 301 (1998) 113.
[119] M. Kardar, Phys. Rep. 301 (1998) 85.
[120] S. Brazovskii, T. Nattermann, Adv. Phys. 53 (2004) 177.
[121] T. Nattermann, V. Pokrovsky, V.M. Vinokur, Phys. Rev. Lett. 87 (2001) 197005.
[122] A.-L. Barabási, H.E. Stanley, Fractal Concepts in Surface Growth. Cambridge University Press, Cambridge, England, 1995.
[123] H. Barkhausen, Z. Phys. 20 (1919) 401.
[124] K.S. Ryu, H. Akinaga, S.C. Shin, Nat. Phys. 3 (2007) 547.

[125] T.J. Yang, V. Gopalan, P.J. Swart, U. Mohideen, Phys. Rev. Lett. 82 (1999) 4106.
[126] G. Catalan, H. Bea, S. Fusil, M. Bibes, P. Paruch, A. Barthelemy, J.F. Scott, Phys. Rev. Lett. 100 (2008) 027602.
[127] B.J. Rodriguez, S. Jesse, A.P. Baddorf, S.H. Kim, S.V. Kalinin, Phys. Rev. Lett. 98 (2007) 247603.
[128] B. Raquet, R. Mamy, J.C. Ousset, Phys. Rev. B54 (1996) 4128.
[129] T.A. Moore, J.A.C. Bland, J. Phys.: Condens. Matter. 16 (2004) R1369.
[130] X. Chen, O. Sichelschmidt, W. Kleemann, O. Petracic, C. Binek, J.B. Sousa, S. Cardoso, P.P. Freitas, Phys. Rev. Lett. 89 (2002) 137203.
[131] S. Lemerle, J. Ferre, C. Chappert, V. Mathet, T. Giamarchi, P. Le Doussal, Phys. Rev. Lett. 80 (1998) 849.
[132] G. Tatara, H. Kohno, Phys. Rev. Lett. 92 (2004).
[133] A. Yamaguchi, T. Ono, S. Nasu, K. Miyake, K. Mibu, T. Shinjo, Phys. Rev. Lett. 92 (2004).
[134] M. Yamanouchi, D. Chiba, F. Matsukura, H. Ohno, Nature 428 (2004) 539.
[135] S.S.P. Parkin, M. Hayashi, L. Thomas, Science 320 (2008) 190.
[136] P. Bak, C. Tang, K. Wiesenfeld, Phys. Rev. A. 38 (1988) 364.
[137] J.P. Sethna, K.A. Dahmen, C.R. Myers, Nature 410 (2001) 242.
[138] S. Zapperi, P. Cizeau, G. Durin, H.E. Stanley, Phys. Rev. B 58 (1998) 6353.
[139] A. Schwarz, M. Liebmann, U. Kaiser, R. Wiesendanger, T.W. Noh, D.W. Kim, Phys. Rev. Lett. 92 (2004).
[140] E. Puppin, Phys. Rev. Lett. 84 (2000) 5415.
[141] E.V. Colla, L.K. Chao, M.B. Weissman, Phys. Rev. Lett. 88 (2002).
[142] R. Nath, Y.-H. Chu, N.A. Polomoff, R. Ramesh, B.D. Huey, Appl. Phys. Lett. 93 (2008) 072905.
[143] N.A. Polomoff, R. Nath, J.L. Bosse, B.D. Huey, J. Vac. Sci. Technol. B27 (2009) 1011.
[144] S. Jesse, B. Mirman, S.V. Kalinin, Appl. Phys. Lett. 89 (2006) 022906.
[145] B.J. Rodriguez, S. Jesse, A.P. Baddorf, S.V. Kalinin, Phys. Rev. Lett. 96 (2006) 237602.